J. Fluid Mech. (2002), *vol.* 450, *pp.* 317–341.
DOI: 10.1017/S0022112001006486 Printed in the United Kingdom

Some observations of the effects of micro-organisms growing on the bed of an open channel on the turbulence properties

By V. I. NIKORA, D. G. GORING AND B. J. F. BIGGS

National Institute of Water and Atmospheric Research, PO Box 8602, Christchurch, New Zealand

(Received 25 July 2000 and in revised form 3 July 2001)

In this paper we report the results of an experimental study of periphyton–flow interactions conducted in a specially designed outdoor hydraulic flume. 'Periphyton' is a collective term for the micro-organisms which grow on stream beds, and includes algae, bacteria, and fungi, with algae usually the dominant and most conspicuous component. The main goals of the study are to identify potential effects of periphyton–flow interactions as well as the potential mechanisms of mass transfer in the near-bed region, which could influence periphyton growth and losses. The main results of the study may be summarized as follows.

A linear velocity distribution in the interfacial sublayer (i.e. below the roughness tops), and a logarithmic distribution above the roughness tops appeared to be reasonable approximations for both flow types, with and without periphyton on the bed. However, the appearance of periphyton on a rough bed shifts the origin of the bed upwards, increases the roughness length z_o by 16–21%, and reduces the ratio of the mean velocity at the level of roughness tops to the shear velocity by $\approx 30\%$. In general, below the roughness tops the periphyton suppresses the mean velocities, the turbulent stresses, turbulence intensities, and vertical turbulent fluxes of the turbulent energy and turbulent shear stresses.

It was found that in flows without periphyton large-scale eddies successfully penetrate the interfacial sublayer. However, tufts of periphyton on the tops of the roughness elements significantly weaken the penetration processes leading to spatial de-correlation in the velocity field within the interfacial sublayer. The appearance of periphyton on the bed does not change appreciably the velocity spectra above the roughness tops but reduces the total spectral energy and generates a wide spectral peak in the interfacial sublayer. Most probably, this peak is formed by penetration of sweep events into the interfacial sublayer, 'filtered' by the periphyton tufts. Thus, sweep events may be the main mechanism responsible for the delivery of nutrients from the outer region to the biologically active interfacial sublayer. The potential effects of flow properties on the periphyton community are also discussed.

1. Introduction

A number of recent studies show that the near-bed hydraulic habitat controls many biological processes determining the functioning of the benthic communities in streams (Biggs & Thomsen 1995; Biggs & Stokseth 1996; Hart & Finelli 1999). Among these communities, periphyton is probably one of the most important components of stream ecosystems, often being the dominant source of energy for higher trophic levels and the

habitat for other organisms. 'Periphyton' is a collective term for the micro-organisms which grow on stream beds. It is this community that gives rocks a slippery feel, and which sometimes forms greenish-brown slimy mats. Periphyton is composed mainly of algae, bacteria, and fungi, with algae usually the dominant and most conspicuous component. Knowledge of mass transfer processes and physical interactions between periphyton and the turbulent stream flow, which control periphyton growth and losses, may become critical to understanding the functioning of natural benthic communities in streams.

Unfortunately, most studies of periphyton–flow interactions have used integral flow measures like the cross-sectional mean velocity, which may provide some useful information but not deep insight into the mechanics of the interactions. Studies in this field of aquatic research lag those of terrestrial canopies (e.g. forest or wheat crops), where for the last 15–20 years the 'air flow–canopy interactions' have been extensively studied both theoretically (e.g. Wilson & Shaw 1977; Raupach & Shaw 1982; Finnigan 1985, 2000) and experimentally (e.g. Raupach, Coppin & Legg 1986; Raupach, Antonia & Rajagopalan 1991; Brunet, Finnigan & Raupach 1994; Finnigan 2000). However, there are two main differences between terrestrial canopies and periphyton mats, which prevent direct use of 'terrestrial' results to describe 'periphyton–flow' interactions. First, periphyton filaments have no rigidity and elasticity and, thus, their response to flow impact should be very different from that found for terrestrial canopies (e.g. Finnigan & Mulhearn 1978). Second, periphyton grows on a rough gravel bed and the thickness h_p of the periphyton mat may be much less than, comparable to, or even larger than the bed roughness height Δ. This is quite different from the terrestrial canopies whose characteristic vertical scales are much larger than the roughness length of the substrate. Indeed, the periphyton effect on flow and vice versa may depend on the species composition, the ratio h_p/Δ, and the filament density. In some cases the periphyton can increase the initial bed roughness (Nikora, Goring & Biggs 1997, 1998*a*) while in other cases it makes the bed smoother (Godillot 1998). At $h_p \gg \Delta$ the roughness elements (e.g. gravel) are completely submerged within the periphyton mat and, most probably, periphyton filaments laminarize the flow below the roughness tops. Because of these complexities, a purely theoretical analysis of the interaction between periphyton and turbulent flow is not at present possible. An experimental approach should be used first to create a conceptual basis for semi-empirical and theoretical models of mass and momentum exchange between the biologically active near-gravel-bed region and the bulk flow. However, some theoretical developments for terrestrial canopies are general enough to be also applicable to the problem of the periphyton–flow interactions. They mainly relate to a methodology based on the time- and spatially-averaged momentum, energy, and transport equations (Wilson & Shaw 1977; Raupach & Shaw 1982; Finnigan 1985; Raupach *et al.* 1991; Finnigan 2000). This relatively new methodology is especially attractive for our study as we are dealing with highly heterogeneous near-bed flow properties due to both bed roughness and periphyton.

The aim of this paper is to report results of an experimental study of the periphyton–flow interactions conducted in a specially designed outdoor eco-hydraulics flume. In this study we attempted to identify potential effects of periphyton–flow interactions as well as the potential mechanisms of mass transfer in the near-bed region, which could influence the periphyton growth and losses. Our approach combines the advantages of both field and laboratory experiments, and is based on the 'spatially averaged' methodology originally developed for the 'air flow–terrestrial canopy' problem (Finnigan 2000) and later adapted for the case of rough-bed open-channel flows (Nikora

et al. 2001). We hope that this paper reduces the gap between terrestrial and aquatic studies and provides a new, interesting example of flow–biota interactions.

2. Experimental design and measurements

2.1. *General*

As we mentioned above, the methodology of this study, including experimental design and data interpretation, is based on the double-averaged (in time and in space) momentum, continuity, and energy equations. It should be noted that we consider steady open-channel flows and, thus, ensemble averaging for our case study may be approximated well by time averaging, at least for practical purposes (Monin & Yaglom 1971). Detailed mathematical analysis as well as a derivation of the double-averaged equations are presented by Rapauch & Shaw (1982), Finnigan (1985), Gimenez-Curto & Corniero Lera (1996), and Finnigan (2000). The double-averaged momentum equations explicitly include several additional terms such as dispersive (form-induced) stresses $\langle \tilde{u}_i \tilde{u}_j \rangle$ due to spatial disturbances in time (ensemble)-averaged flow and the form drag on the rough bed. Here and in what follows the overbar and angle brackets denote the time (ensemble) and spatial average of flow variables, respectively; the tilde denotes the disturbance in the flow variables, i.e. the difference between time-averaged ($\bar{\mathscr{V}}$) and double-averaged ($\langle \bar{\mathscr{V}} \rangle$) values, ($\tilde{\mathscr{V}} = \bar{\mathscr{V}} - \langle \bar{\mathscr{V}} \rangle$), similar to the Reynolds decomposition ($\mathscr{V}' = \mathscr{V} - \bar{\mathscr{V}}$). The double-averaged energy equations also contain some additional terms such as a wake production term P_w (i.e. energy generation in wakes behind roughness elements or plants, $P_w \approx -\langle \bar{u} \rangle \partial \langle \overline{u'w'} \rangle / \partial z$), and some others (Kaimal & Finnigan 1994; Finnigan 2000).

Based on double-averaged equations, an open-channel flow with a hydraulically rough bed may be subdivided into the following specific regions (Nikora *et al.* 2001): (i) the outer layer where the viscous effects and dispersive stresses are negligible and the double-averaged equations are identical to the time (ensemble)-averaged equations; (ii) the logarithmic layer (if the flow depth is sufficiently larger than the roughness height, Raupach *et al.* 1991); (iii) the dispersive (form-induced) sublayer, just above the roughness crests, where the flow may be influenced by individual roughness elements and, thus, the term $\langle \tilde{u}_i \tilde{u}_j \rangle$ may be important; and (iv) the interfacial sublayer which is also influenced by individual roughness elements and occupies the flow region between roughness crests and troughs. A new important term in the interfacial sublayer is form drag. The dispersive and interfacial sublayers together may be identified as the roughness layer. Thus, in our study we tried to measure and interpret both time-averaged and double-averaged variables.

2.2. *Equipment*

Experiments were conducted in an outdoor, tilting hydraulic flume specially designed for studies of flow–biota interactions (Nikora, Goring & Biggs 1998*b*). The flume, 12 m long by 75 cm wide, is situated on the left bank of the Kaiapoi River, 30 km north of Christchurch (NIWA Silverstream Research Facility), New Zealand. The flume bed and walls are made of transparent acrylic plates. Depending on experimental design, the flume can be run using two working regimes: (i) closed re-circulation; or (ii) open circulation with water supplied from the Kaiapoi River passing through the flume and released back into the river at the end of the flume. This outdoor facility successfully combines two contrasting features: (i) near-field conditions (light, natural water, nutrients, seeding material, etc.), which are crucial for flow–biota interaction studies and which cannot be achieved in a conventional laboratory; and (ii) detailed

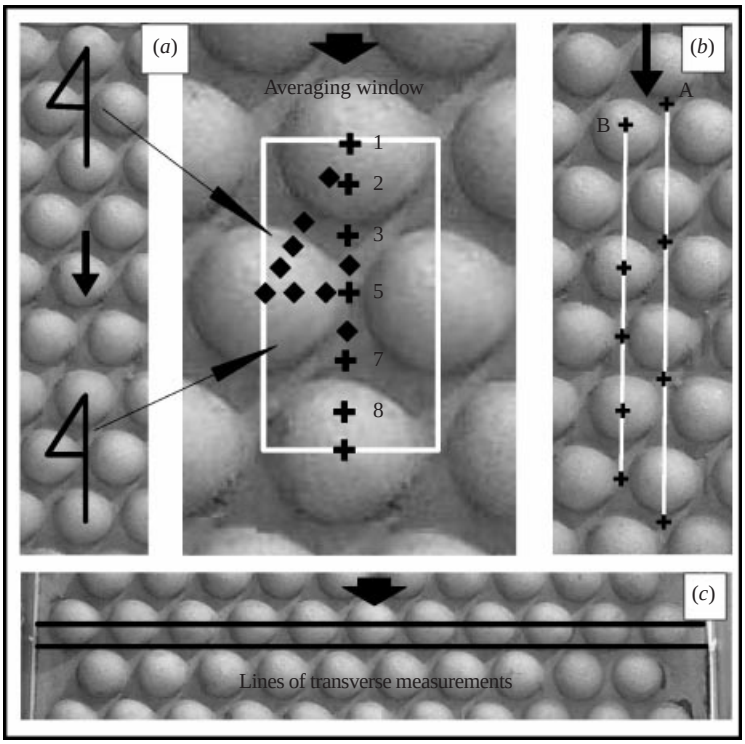

FIGURE 1. Bed roughness pattern and horizontal positions of the ADV measurement points for sets 1 (*a*), 2 (*b*), 3 (*c*). The numbers in (*a*) correspond to the numbers in figure 13. The spherical segments, 60 mm in chord, may serve as the scale.

control and manipulation of hydraulic variables typical of hydraulic and aquatic laboratories. Detailed information and hydraulic tests of the flume may be found in Nikora *et al.* (1998*b*). For the reported experiments, the flume bed was completely covered by 1.2 mm thick styrene sheets with thin (0.3–0.4 mm) flocked ('velvet') coating with spherical segments, 60 mm in chord and $\Delta = 21$ mm in height. The roughness pattern for this rough bed is shown in figure 1. The same 'velvet' coating, but without spherical segments, was used for the original hydraulic tests of this flume (Nikora *et al.* 1998*b*). In previous studies (e.g. Biggs & Thomsen 1995) it was shown that such a rough surface provides effective conditions for colonization and growth of periphyton.

The three-dimensional velocities were measured with two down-looking and one up-looking SonTek's Acoustic Doppler Velocimeters (ADVLab, Kraus, Lohrmann & Cabrera 1994; Lohrmann, Cabrera & Kraus 1994; Nikora & Goring 1998*a*; Voulgaris & Trowbridge 1998). An important advantage of the ADV is that it measures water flow in a small sampling volume (0.25 cm^3), 5 cm away from the sensing elements. Since down-looking ADV sensors do not permit measurements near the water surface they were supplemented with an up-looking ADV probe to cover the near-surface region. The probes were mounted in a specially designed frame equipped with a stepper motor and installed into the instrumental carriage. This ensured a high level of accuracy in positioning probes over the bed ($\pm$0.2 mm) and along/across the flume ($\pm$1.0 mm).

Parameter	Experimental runs			
	LF	HF	LFP	HFP
Flow rate $Q\,(\mathrm{l\,s^{-1}})$	48.9	92.0	47.1	93.0
Cross-sectional mean velocity $U_a\,(\mathrm{cm\,s^{-1}})$	52.0	71.1	53.2	70.6
Cross-sectional mean depth $H_a\,(\mathrm{cm})$	12.55	17.25	11.82	17.57
Maximum depth H_m (cm)	13.46	18.16	13.10	18.85
Hydraulic radius R (cm)	9.40	11.82	8.99	11.96
Width to depth ratio (B/H_a)	5.98	4.35	6.34	4.27
Bed slope S_b	0.00320	0.00310	0.00320	0.00310
Water surface slope S_w	0.00403	0.00466	0.00404	0.00483
Energy slope $S_e = S_b - \mathrm{d}H_a/\mathrm{d}x - \mathrm{d}(U_a^2/2g)/\mathrm{d}x$	0.00385	0.00419	0.00384	0.00433
Reynolds number $Re = U_a H_a/\nu$	65260	122648	62882	124044
Karman number $Ka = u_* H_a/\nu$	8154	13288	7646	13709
Froude number $Fr = U_a/\sqrt{gH_a}$	0.468	0.547	0.494	0.538
Roughness Reynolds number $Re_* = u_*\delta/\nu$	1365	1617	618	858
Non-uniformity parameter $\beta = -S_w/S_e$	−1.05	−1.11	−1.05	−1.12
Global shear velocity $u_{*g} = \sqrt{gRS_e}\,(\mathrm{cm\,s^{-1}})$	5.96	6.97	5.82	7.13
Gravity term $\sqrt{gH_aS_e}\,(\mathrm{cm\,s^{-1}})$	6.88	8.42	6.67	8.64
[a]Mean bed shear velocity $\bar{u}_{*b}\,(\mathrm{cm\,s^{-1}})$	6.58	7.78	6.37	7.96
'Stress' bed shear velocity $u_{*s}\,(\mathrm{cm\,s^{-1}})$	6.50	7.60	6.40	7.60
'Log' bed shear velocity $u_{*l}\,(\mathrm{cm\,s^{-1}})$	6.41	7.73	6.64	7.91
Shear velocity $u_* = (\bar{u}_{*b} + u_{*s} + u_{*l})/3\,(\mathrm{cm\,s^{-1}})$	6.5	7.7	6.5	7.8
$C = \langle\bar{u}\rangle(\delta)/u_*$	7.1	7.1	5.0	5.0
'Log' roughness length $z_o\,(\mathrm{cm})$	0.115	0.122	0.146	0.142
Displacement length $d\,(\mathrm{cm})$	0.00	0.00	1.15	1.00
[b]Roughness height $\delta = \Delta - d\,(\mathrm{cm})$	2.10	2.10	0.95	1.10
Relative roughness (δ/H_m)	0.156	0.116	0.073	0.058

TABLE 1. Background conditions of the experiments (mean values from repeated measurements are shown). [a] $\bar{u}_{*b} = \sqrt{gH_aS_e - (2H_m/B)u_{*w}^2}$ where the sidewall shear stress u_w^2 was obtained using an empirical relationship $u_w^2 = f(gH_aS_e, B/H_a)$ in Nezu & Nakagawa (1993, p. 94); [b] Δ is the height of the spherical segments on the bed ($\Delta = 2.1$ cm). LF and HF are low and high flows without periphyton, respectively; and LFP and HFP are low and high flows with periphyton, respectively.

2.3. *Experimental design*

First, measurements were made at two flow rates (table 1) using the closed re-circulation regime with tap water, to prevent colonization and growth of periphyton on the bed. These two flow rates will be further referred to as 'high' (HF) and 'low' (LF) flows. According to Nikora *et al.*'s (2001) classification, both flows may be identified as flows with high relative submergence. When the first stage was completed, the flume set-up was changed to the open circulation ('once through the system') with the high flow rate, and the flume was left running for 18 days for colonization and growth of periphyton on the bed. During this period the periphyton growth comprised several stages. By the end of the first week the colonisation of the flume was completed, and periphyton covered the bed surface uniformly, with approximately the same thickness (1–2 mm) on the spherical segments and between them. Then, during the second week, transverse strips of quickly growing periphyton appeared on the roughness elements, and by the end of the week their tops were covered with tufts of periphyton that resembled forelocks in appearance (figure 2). The thickness of these 'forelocks' was approximately 3 to 5 mm and remained the same during the next few days. The

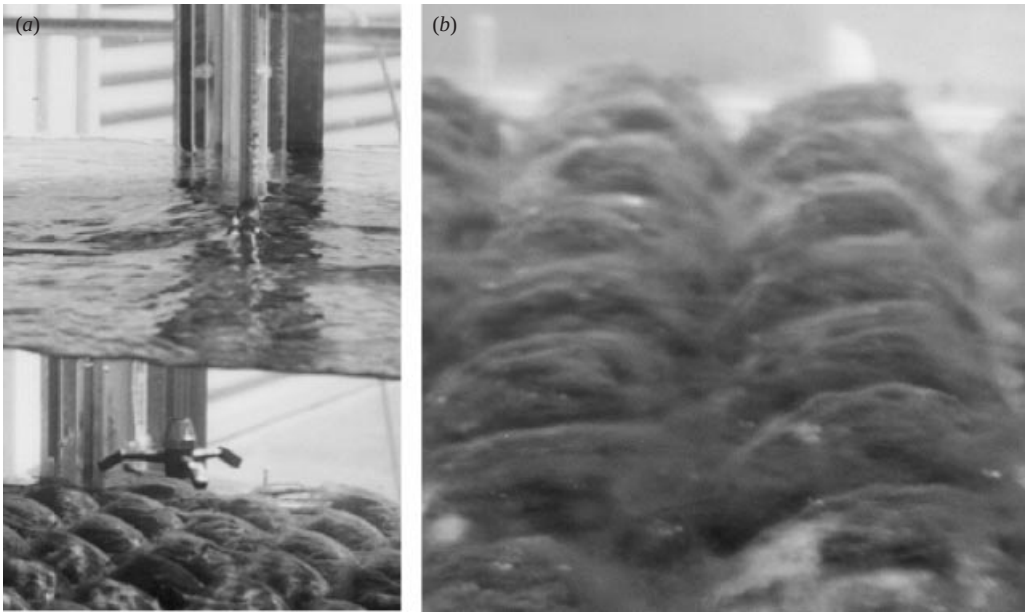

FIGURE 2. An example of (*a*) an experimental set-up, and (*b*) periphyton 'forelocks' on the spherical segments from figure 1.

dominant species of the periphyton community were the diatom *Synedra* and the green filamentous *Spirogyra*. With the appearance of the 'forelocks' the periphyton mat between the spherical segments became unstable, the mat thickness was reduced, and the periphyton mat between the roughness elements became patchy. At this stage it was decided that periphyton on the bed was well developed and growth in the periphyton biomass had saturated, so the ADV measurements were repeated at the same two flow rates as before without periphyton (first at high flow, HFP, and then at low flow, LFP, table 1). Such a design allowed us to unambiguously identify the periphyton effects on the flow and vice versa. Also, in addition to LF/LFP and HF/HFP, bulk flow measurements (flow depths and water surface slopes) were made for a wide range of flow rates at both stages with and without periphyton (from 17 to 162 $\mathrm{l\,s^{-1}}$ for stage 1 and from 21 to 117 $\mathrm{l\,s^{-1}}$ for stage 2).

We chose a free-fall condition at the flume exit, i.e. there was no traditional weir. This prevented any potential blocking of the exit structure by periphyton material, and achieved long-term flow stability. All ADV measurements were made within a section 4.7 to 5.2 m from the flume entrance where the flow was found to be completely developed (Nikora *et al.* 1998*b*). This agrees well with estimates based on a semi-empirical relationship $X_H = (H_a/\gamma)(U/u_*)$ for hydraulically rough beds (Monin & Yaglom 1971, pp. 323, 324; 1992, pp. 283, 284), where X_H is the distance required for the flow to be fully developed, H_a is the mean flow depth, U is the free-stream velocity, u_* is the shear velocity, and $\gamma = 0.33$ is a coefficient. According to this relationship a fully developed flow should be achieved at $X \approx 3.4$ m for LF and LFP, and at $X \approx 4.0$ m for HF and HFP. In our study we used the right-handed coordinate system, with the x-axis oriented along the flume (u-velocity component), the y-axis oriented towards the left bank (v-velocity component), and the z-axis oriented toward the water surface with its origin at the bed surface, i.e. at the base of the roughness elements (w-velocity component).

Three identical sets of velocity measurements were conducted at each stage and at each flow rate:

1. The measurements were made at seven verticals positioned along the flow and covering one wavelength of roughness elements (figure 1*a*, crosses), with 16 (LF) to 22 (HF) measuring points at each vertical. Two identical patterns, as shown in figure 1(*a*), were measured simultaneously with a distance between them of 30.7 cm. Both patterns were positioned at $b/B = 0.6$, where b is the distance from the right wall of the flume, and B is the flume width. For LF the measurements were also taken at nine additional verticals (figure 1*a*, diamonds). This set of measurements was aimed at studying the vertical distribution of turbulence properties, their heterogeneity introduced by the roughness elements and the patchy periphyton mat, and potential effects of non-uniformity. The measurement set thus obtained is defined as data set 1.

2. The second set included two subsets, A and B, of synchronous measurements in seven pairs of verticals with 10 (A) and 6 (B) measuring points in each. The positions of the upstream verticals were kept the same for each pair. The measurements of subset A (figure 1*b*) covered the flow region from $z = 0.4$ cm to $z = 4.0$ cm, i.e. it includes the interstitial space between roughness elements. The subset B (figure 1*b*) covers the layer from roughness tops to $z = 4.0$. The aim of this set was to explore spatial correlations in the velocity field, and the roughness and periphyton effects on these correlations. This is defined as data set 2.

3. Measurements were made in the transverse direction across the flume at $z \approx 2.8$ cm and ≈ 0.8 cm below the water surface, with spatial intervals $\Delta y = 0.5$ cm or $\Delta y = 1$ cm. These measurements were made over both roughness tops and troughs (figure 1*c*). We used these measurements to identify roughness effects on small-scale heterogeneity in turbulence structure, and to detect and quantify possible secondary currents, if any. This is defined as data set 3.

For all velocity data sets, the duration of the measurements at each point was 1 min with the sampling frequency of 100 Hz, as previous work had shown that these parameters provide stable statistical characteristics (Nikora *et al.* 1998*b*). All measurements were conducted in accordance with the technical routines recommended in the ADV manual and also developed in Nikora & Goring (1998*a*) and Voulgaris & Trowbridge (1998).

To control background conditions, the flow rate, flow depths (at every 0.6 m along the flume), water temperature, piezometer levels, and weather conditions were recorded each 40–50 min during the measurements. The nutrient concentrations (phosphorus, etc.) at the flume intake, the periphyton biomass, and longitudinal profiles of the flume bed were monitored daily. The latter was necessary to detect and eliminate potential micro-deformations of the flume due to changeable weather conditions (Nikora *et al.* 1998*b*). Table 1 presents the background conditions of the experiments related to the working section where the flows investigated may be characterized as slightly accelerating, steady, nearly equilibrium flows.

2.4. *Data analysis*

The analysis of the velocity data set (more than 2000 single-point ADV files or 6000 velocity time series) comprised three stages. In stage 1 the data were extracted from the initial binary files and checked for unreliable records. About 18% of the ADV files were rejected as unreliable because of a high level of Doppler noise, interference with the bed, etc. (Nikora & Goring 1998*a*; Voulgaris & Trowbridge 1998). Then, in stage 2, to minimize errors in turbulence characteristics related to the sensor misalignment (that may cause leakage of the longitudinal velocity component into the other two

components), velocity records were corrected. A three-step procedure was applied which is based on the assumption that in the central part of the flume the flow well above the bed and still far from the water surface is close to two-dimensional. First, the mean velocity vector was rotated in the (x, y)-plane to reduce the mean transverse velocity to zero. Second, a similar procedure was applied in the (x, z)-plane to reduce the mean vertical velocity to zero. Finally, the axes were rotated in the (y, z)-plane to reduce the moment $\overline{v'w'}$ to zero. This three-step procedure provided three misalignment angles for each sensor at each selected point in the central, two-dimensional part of the flume. Then, the angles were averaged and used to correct velocity at all points within a measurement set. In most cases the misalignment angles did not exceed 2°. In stage 3, the corrected velocity data were used to calculate various turbulence characteristics using the ADVANS package (Goring, Nikora & Brown 1998) specially developed for various turbulence analyses from ADV data.

3. Vertical structure of turbulence in the central quasi-two-dimensional part of the flow

3.1. *Velocity distribution*

Nikora *et al.* (2001) suggested a simplified three-layer model, which neglects potential transitional effects in the dispersive sublayer, and thus comprises three layers: (i) an outer layer; (ii) a logarithmic layer; and (iii) a linear or interfacial sublayer. This simplified model is similar to the two-layer Prandtl model for smooth-bed flows (Monin & Yaglom 1971), which neglects the transitional effects in the buffer sublayer. Applying a re-formulation of Izakson's (1937) overlap approach (also described by Millikan 1939) for double-averaged velocity $\langle\bar{u}\rangle$ Nikora *et al.* (2001) obtained for the logarithmic layer:

$$\frac{\langle\bar{u}\rangle}{u_*} = \frac{1}{\kappa}\ln\left[\frac{z-d}{\delta}\right] + C = \frac{1}{\kappa}\ln\left[\frac{z-d}{z_o}\right] \quad \text{for} \quad z \geqslant \Delta, \tag{1}$$

where κ is the von Kármán constant, z is the distance from the flume bed (it serves as support for the spherical segments), δ is the thickness of the interfacial sublayer, d is the displacement length (also known as a zero-plane displacement), $z_o = \delta\exp(-\kappa C)$ is the roughness length, and $C = \langle\bar{u}\rangle(\delta)/u_*$ should depend on the roughness geometry. We define δ as the distance between the roughness tops and the position of the bed origin where $z-d=0$ and $\langle\bar{u}\rangle(d)=0$, i.e. $\delta = \Delta - d$. Note that relationship (1) for the double-averaged velocity $\langle\bar{u}\rangle$ extends the standard logarithmic layer for $\bar{u}$ down to the roughness crests. Also, using an analogy with the viscous sublayer for smooth-bed flows, Nikora *et al.* (2001) derived a linear relationship for the interfacial sublayer:

$$\frac{\langle\bar{u}\rangle}{u_*} = C\frac{z-d}{\delta} \quad \text{for} \quad z \leqslant \Delta. \tag{2}$$

Relationships (1) and (2) are supported by a number of laboratory (Nikitin 1963, 1980; Dittrich & Koll 1997) and field (Griffiths 1981; Bray 1985) studies, and, therefore, we use these relationships as a basis to study effects of periphyton–flow interactions on the velocity distribution in our rough-bed flume. Figures 3(*a*) and 3(*b*) show vertical distributions of local time-averaged velocities from data sets 1 and 2 (figure 1). Three conclusions may be drawn from these figures. First, the near-bed local time-averaged velocities vary by 20–50% at any given distance from the bed for both flow types, with and without periphyton. The dispersion of data points is much

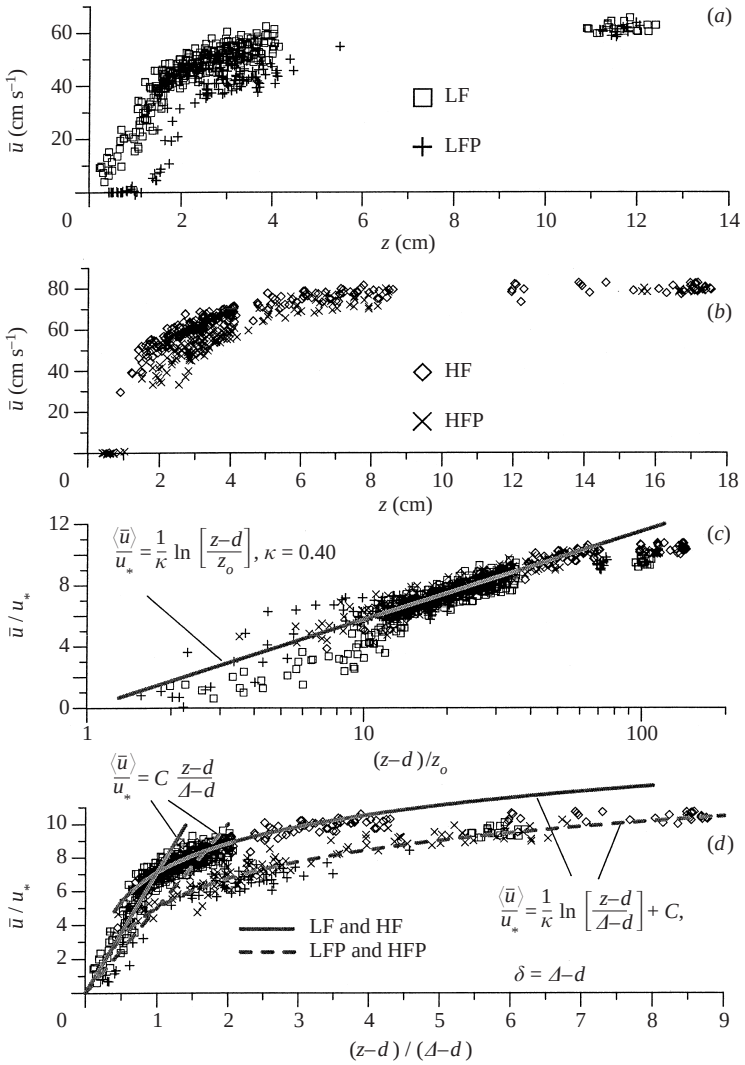

FIGURE 3. Vertical distribution of the mean longitudinal velocity: (*a*) and (*b*) are for the low and high flows, respectively; (*c*) and (*d*) are the data approximation with relationships (1) and (2).

larger than the errors in time-averaged velocities ($< 1\%$) and, therefore, it should be attributed to the effects of local conditions on the bed. The strong heterogeneity in local mean velocities supports the necessity of double averaging, which we use as the main methodology in this study. Second, the displacement length d changes from zero for the flows without periphyton to approximately 1 cm for flows with periphyton on the bed (table 1). Third, the linear approximation for the velocity distribution within the interfacial sublayer is not unreasonable. Figure 3(*c*) compares our measurements with relationship (1) and shows that the log formula is applicable within the range of $(z - d)/z_o$ from $\approx$ 14 to 70, with the same value for the von Kármán constant as for the time-averaged velocity distribution in two-dimensional flows far away from the roughness elements, i.e. $\kappa = 0.40$. Another useful representation of the data is shown in figure 3(*d*) where both relationships (1) and (2) are compared with the measurements. The solid and dashed lines in this figure represent the double-averaged

(in time and in space) velocities, while table 1 gives the parameters for (1) and (2) based on best-fit approximations. Note that here and in the following sections we use for normalizations the shear velocity u_* obtained as the mean of three independent estimates (u_{*l} from the log profile, u_{*s} from the Reynolds stress measurements, and $\bar{u}_{*b}$ from the bulk flow measurements, table 1). Although relationships (1) and (2) appeared to be reasonably valid for both flow types (with and without periphyton), the data for these flows collapsed around different curves (figure 3*d*). Thus, the appearance of periphyton on a rough bed shifted the origin of the bed upwards, increased the roughness length by 16–21%, and reduced $C = \langle\bar{u}\rangle(\delta)/u_*$ by $\approx 30\%$. The effect of the flow rate on these parameters appeared to be insignificant (table 1).

3.2. *Distribution of turbulent and dispersive shear stresses*

For two-dimensional, uniform, double-averaged rough-bed flow one can obtain the following relationships for the shear stresses (Nikora *et al.* 2001):

the dispersive sublayer and logarithmic layer

$$[-\langle\overline{u'w'}\rangle(z) - \langle\tilde{u}\tilde{w}\rangle(z)] \approx -\langle\overline{u'w'}\rangle(z) \approx gS_b[z_{ws} - z] = u_*^2[(z_{ws} - z)/H_a]; \qquad (3)$$

the interfacial sublayer

$$[-A\langle\overline{u'w'}\rangle(z) - A\langle\tilde{u}\tilde{w}\rangle(z)] \approx -A\langle\overline{u'w'}\rangle(z) \approx gS_b\left\{z_{ws} - z_c + \int_z^{z_c} A(z)\,\mathrm{d}z\right\} - \int_z^{z_c} \frac{A(z)}{\rho}\left\langle\frac{\partial\tilde{p}}{\partial x}\right\rangle \mathrm{d}z, \qquad (4)$$

where g is the acceleration due to gravity, S_b is the bed slope, z_{ws} is the water surface elevation, z_c is the elevation of the roughness crests, A is the ratio of the area A_f occupied by fluid to the total area A_o of the averaging region ($A \equiv 1$ for $z > z_c$ and $A < 1$ for $z < z_c$), H_a is the mean depth, and p is pressure. The last term in (4) describes the form drag. From equation (3) it follows that for the region above the roughness crests in the dispersive sublayer and the logarithmic layer the gravity force $gS_b[z_{ws} - z]$ is balanced by the turbulent and dispersive shear stresses. To balance the gravity force below the roughness crests in the interfacial sublayer the turbulent and dispersive stresses are supplemented with the form drag, equation (4). The double-averaged stresses $-\langle\overline{u'v'}\rangle$ and $-\langle\overline{v'w'}\rangle$ should be equal to zero if the double-averaged flow is uniform and two-dimensional, although the local shear stresses $-\overline{u'v'}$ and $-\overline{v'w'}$ may deviate from zero significantly due to flow heterogeneity in the near-bed region (Nikora *et al.* 2001).

Estimates of the dispersive stresses $-\langle\tilde{u}\tilde{w}\rangle$ showed that they are less than 5–6% of $-\langle\overline{u'w'}\rangle$, being largest at the level of the roughness tops and negligible away from that level. Thus, neglecting them in equations (3) and (4) is reasonable. The distributions of the normalized Reynolds shear stresses $-\langle\overline{u'w'}\rangle/u_*^2$, $-\langle\overline{u'v'}\rangle/u_*^2$, and $-\langle\overline{v'w'}\rangle/u_*^2$ for our experiments are presented in figure 4. As with the mean velocities, the scatter of the local stresses $-\overline{u'w'}$, $-\overline{u'v'}$ and $-\overline{v'w'}$ is much larger than the errors in their estimates ($< 5\%$) and, therefore, it should be attributed to the flow heterogeneity. In general, these distributions deviate from those predicted for two-dimensional uniform flows, equation (3). Indeed, $-\langle\overline{u'w'}\rangle/u_*^2$ changes nonlinearly at $z > z_c$ and $-\langle\overline{u'v'}\rangle/u_*^2$ is non-zero for $[(z - d)/(\Delta - d)] > 3.5$. These effects may be explained by the effects of flow non-uniformity and/or secondary currents (see § 4 for details). Slightly above and below the roughness tops in the central part of the flume, the potential effects of flow non-uniformity and/or secondary currents should

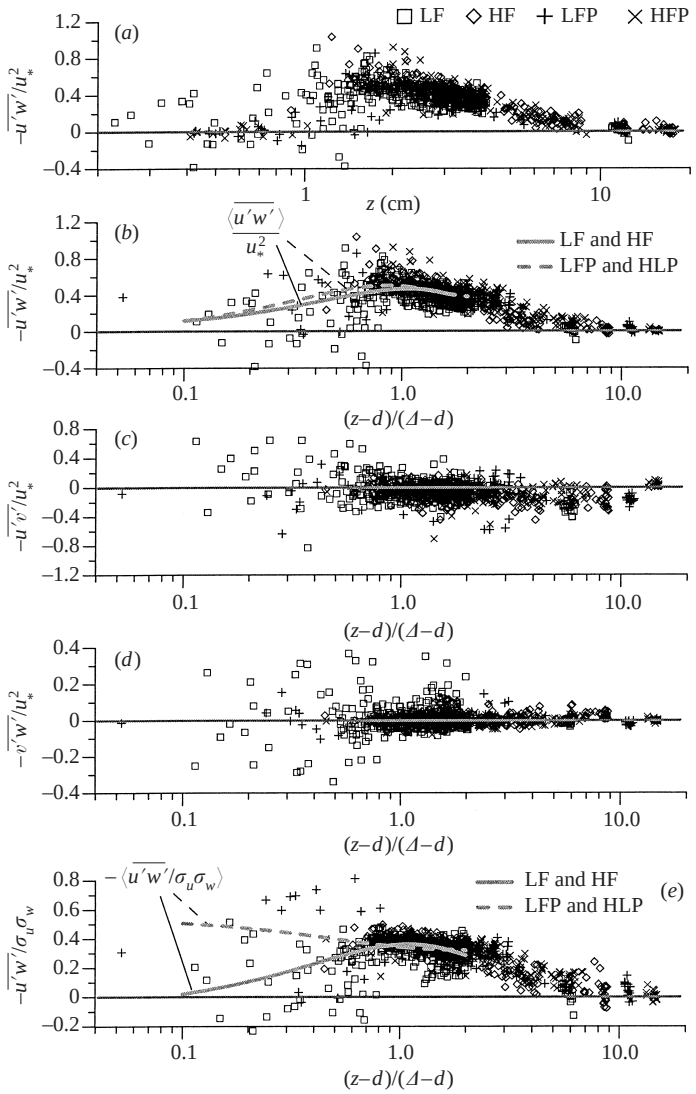

FIGURE 4. Vertical distribution of the turbulent shear stresses: (*a*) and (*b*) are for the primary stress $-\overline{u'w'}$; (*c*) and (*d*) are for $-\overline{u'v'}$ and $-\overline{v'w'}$, respectively; and (*e*) is for the correlation coefficient $-\overline{u'w'}/\sigma_u\sigma_w$.

be negligible, and, therefore, we used extrapolation of $-\langle\overline{u'w'}\rangle$ from the region above the roughness tops towards the mean bed (see equation (3)) to obtain estimates of the bed shear stress and shear velocity u_{*s}. These estimates appeared to be very close to those obtained from other methods (table 1), in spite of neglecting $-\langle\tilde{u}\tilde{w}\rangle$ and the high level of uncertainties involved in the extrapolation of $-\langle\overline{u'w'}\rangle$. In flows with periphyton on the bed the shear stress $-\langle\overline{u'w'}\rangle$ attains a maximum at the level of roughness tops, then, in agreement with (4), gradually reduces towards the bed, and approaches zero approximately 1 cm from the bed (figure 4*a*). The shear stress $-\langle\overline{u'w'}\rangle$ in flows without periphyton behaves similarly except that it approaches zero at $z < 1$ cm. These results agree well with velocity observations and estimates of the displacement length d obtained in the previous section. The presentation of data in

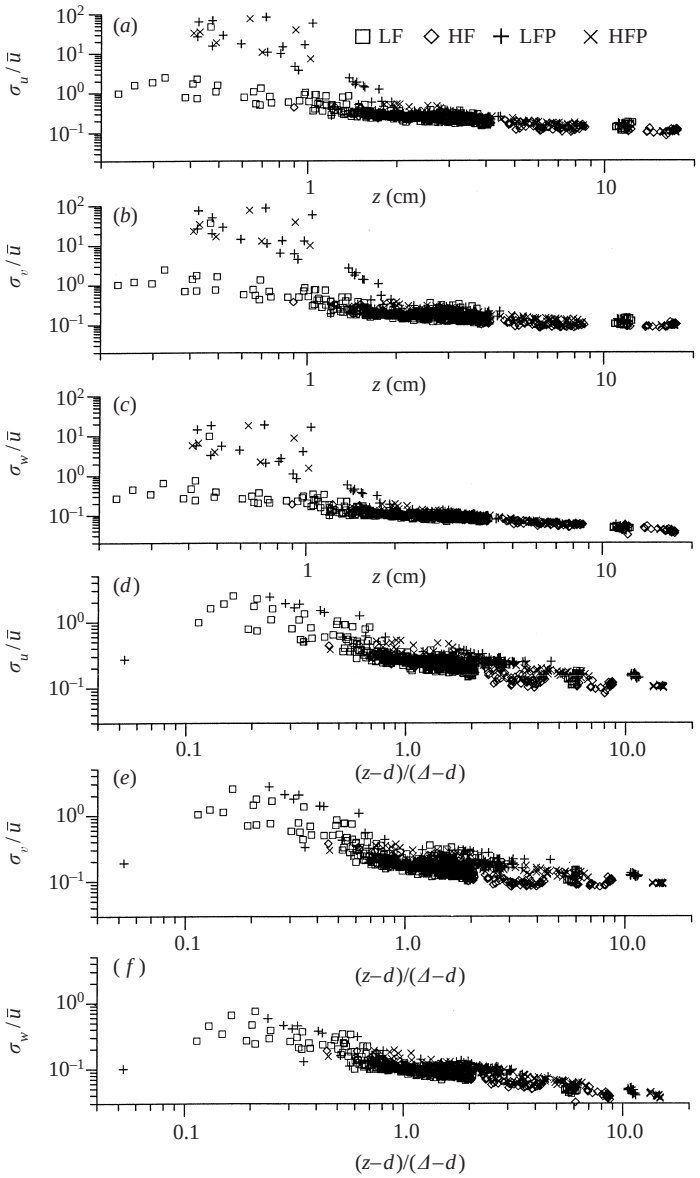

FIGURE 5. Vertical distribution of the relative turbulence intensities: (*a*)–(*c*) $\sigma_i/\bar{u} = f(z)$; and (*d*)–(*f*) $\sigma_i/\bar{u} = f[(z-d)/(\Delta-d)]$.

coordinates $\{-\langle\overline{u'w'}\rangle/u_*^2$ vs. $(z-d)/(\Delta-d)\}$ eliminates this difference (figure 4*b*). There were no appreciable differences in the distributions of $-\langle\overline{u'v'}\rangle$ and $-\langle\overline{v'w'}\rangle$ between the two flow types (figures 4*c* and 4*d*). The correlation coefficient $-\overline{u'w'}/\sigma_u\sigma_w$ for both flow types, with and without periphyton, increases towards the bed, reaches a maximum at the level of roughness tops, and then behaves differently, being larger for flows with periphyton on the bed (figure 4*a*). The results of this and the previous section allowed us to make approximate estimates of the wake production term $P_w \approx -\langle\bar{u}\rangle\partial\langle\overline{u'w'}\rangle/\partial z$. They appeared to be comparable with the shear production term $P_s \approx -\langle\overline{u'w'}\rangle\partial\langle\bar{u}\rangle/\partial z$, i.e. $P_w \approx P_s$ for both flow types.

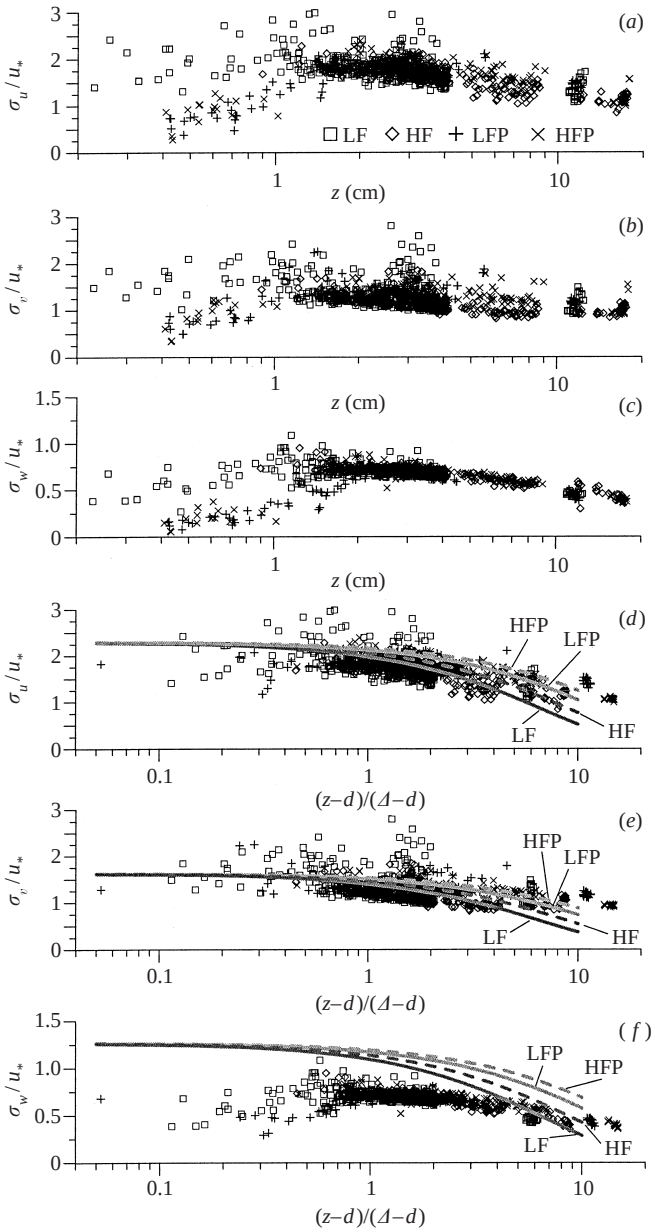

FIGURE 6. Vertical distribution of the relative turbulence intensities: (*a*)–(*c*) $\sigma_i/u_* = f(z)$; and (*d*)–(*f*) $\sigma_i/u_* = f[(z-d)/(\Delta-d)]$. The solid and dashed lines are approximations suggested for open-channel flows in Nezu & Nakagawa (1993).

3.3. *Turbulence intensities*

In our study we analysed two types of relative turbulence intensities, normalizing the velocity standard deviations with the local mean longitudinal velocity (i.e. $\sigma_i/\bar{u}$, figure 5), and with the shear velocity (i.e. σ_i/u_*, figure 6). Figures 5 and 6 show that above the roughness tops the data points for low and high flows, with and without periphyton, collapse within fairly narrow bands. This statement is valid for both

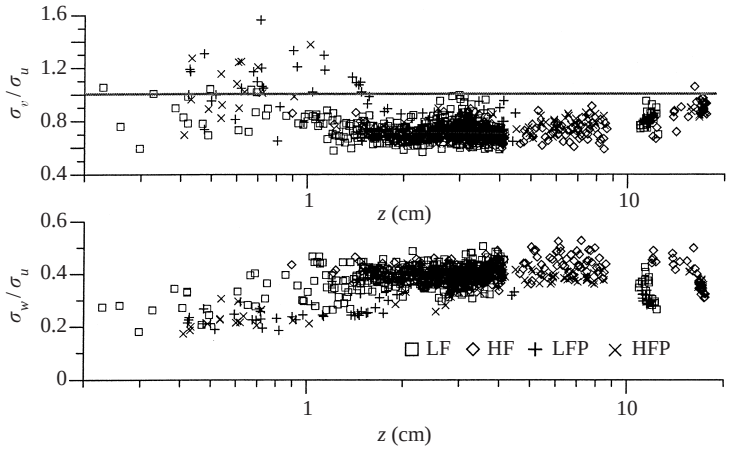

FIGURE 7. Vertical distribution of the 'anisotropy' ratios σ_v/σ_u, $\sigma_w/\sigma_u = f(z)$.

types of data presentation, as a function of z and as a function of $(z-d)/(\Delta-d)$. However, below the roughness tops the relative turbulence intensities $\sigma_i/\bar{u}$ are much higher (figure 5*a–c*) while σ_i/u_* are much lower (figure 6*a–c*) for the 'periphyton' flows, compared with $\sigma_i/\bar{u}$ and σ_i/u_* for flows without periphyton on the bed. Thus, although the periphyton on the bed suppress both the mean velocities $\bar{u}$ and the turbulence intensities σ_i, the suppression of $\bar{u}$ was stronger than that of σ_i, and this explains such behaviour in the distributions of $\sigma_i/\bar{u}$ and σ_i/u_* in the interfacial sublayer. Furthermore, the suppression of the turbulence intensities σ_i by periphyton was different for different velocity components. Figure 7 shows that the ratios σ_v/σ_u and σ_w/σ_u at $z < \Delta$ for 'periphyton' flows appeared to be different from those for flows without periphyton. An explanation for this difference is that the intensity σ_w was suppressed more than σ_u while the σ_v was suppressed less than σ_u, as can be deduced from figures 5, 6, and 7. The replacement of z with $(z-d)/(\Delta-d)$ in figures 5(*d–f*) and 6(*d–f*) eliminates the differences between the two flow types noted in figure 5(*a–c*) and 6(*a–c*). Figure 6(*d–f*) compares our measurements with the exponential-type relationships for σ_i/u_* suggested in Nezu & Nakagawa (1993) for open-channel flows. These relationships describe our data fairly well, even very close to the bed, except for the vertical velocity component (figure 6*f*).

3.4. *High-order moments*

High-order velocity moments provide additional information on the shape of the velocity distribution, which supplement the results for the mean velocities, turbulence intensities, and turbulent shear stresses. Besides, the n-order moments have a clear physical meaning as the fluxes of $(n-1)$-order moments. For instance, the third-order moments describe fluxes of the Reynolds tensor components, providing important information on the turbulent transport terms in the turbulent kinetic energy and shear stress balance (Raupach *et al.* 1991). We first present the skewness ($Sk_i = \overline{u_i'^3}/\sigma_i^3$) and kurtosis $Ku_i = (\overline{u_i'^4}/\sigma_i^4) - 3$ coefficients (figure 8). The skewness Sk_v for the transverse velocity is close to zero, on average, for most of the depth, as one would expect for two-dimensional flow. However, this is not the case for Sk_u and Sk_w, which look like reflections of each other. Indeed, they both change sign at the level of the roughness tops, i.e. at $[(z-d)/(\Delta-d)] \approx 1$: $Sk_u > 0$ and $Sk_w < 0$ below the roughness tops and $Sk_u < 0$ and $Sk_w > 0$ above. This property indicates that the prevailing transport of

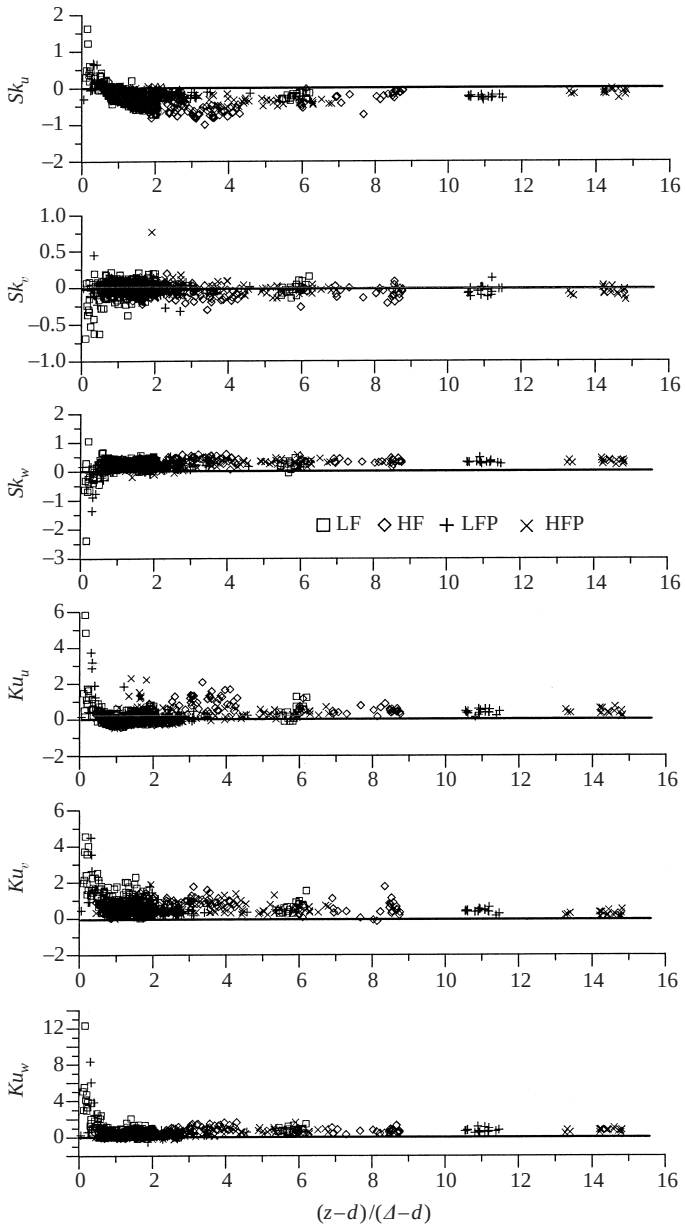

FIGURE 8. Vertical distribution of the skewness and kurtosis coefficients for the velocity components u, v, and w.

the turbulent energy below the roughness tops occurs toward the flume bed, while above them the energy is transported upwards. A similar behaviour of Sk_u and Sk_w was reported in Nikora & Goring (2000*a*) for rough-bed open-channel flows and in Raupach *et al.* (1986) for the air flow inside and above a model plant canopy in a wind tunnel. The distributions of the kurtosis coefficients for all three velocity components are similar: they are positive above the roughness tops, tend to be zero around the roughness top level, and increase again towards the flume bed (figure 8). Interestingly, the kurtosis Ku_w near the bed is appreciably higher than Ku_u and Ku_v,

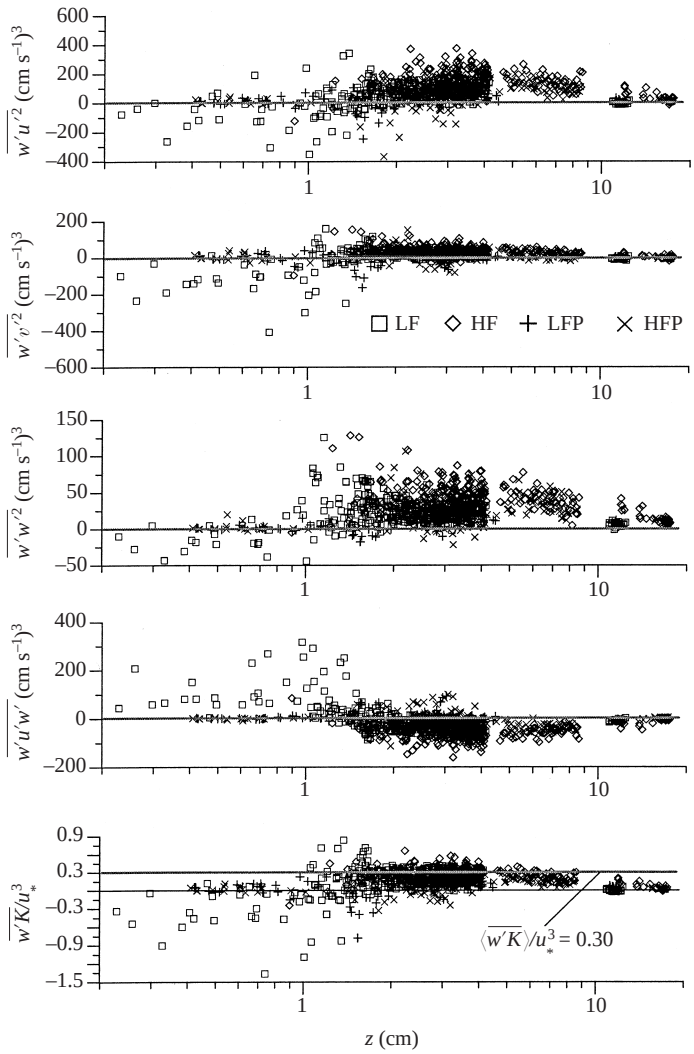

FIGURE 9. Vertical distribution of the mixed third-order moments describing the vertical flux of the turbulent energy.

which reflects the high level of intermittency in the vertical mass exchange between the interfacial sublayer and the logarithmic layer. A similar result was reported for the flow inside and above a model canopy (Raupach *et al.* 1986). Figure 8 provides no evidence of periphyton effects on Sk_i and Ku_i, just like figures 5(*d–f*) and 6(*d–f*) where the coordinate $(z-d)/(\Delta-d)$ was used. However, the effects of periphyton are evident in figure 9, which shows the vertical distributions of the moments $\overline{u'^2w'}$, $\overline{v'^2w'}$, $\overline{w'^3}$, $\overline{w'K}$ and $\overline{u'w'^2}$, without normalization (except $\overline{w'K}$) and using z instead of $(z-d)/(\Delta-d)$ used in figure 8. These moments characterize vertical turbulent transport of the energy of the velocity components ($\overline{u'^2}$, $\overline{v'^2}$, $\overline{w'^2}$), the total turbulence energy $K = 0.5(\overline{u'^2}+\overline{v'^2}+\overline{w'^2})$, and the shear stress $\overline{u'w'}$. For the 'periphyton' flows these transport terms are negligible below $z \approx 1$ cm, being noticeably different from the 'non-periphyton' flows, where the transport terms are significantly non-zero in this flow region. Recall that $z \approx 1$ corresponds to the position of the bed origin for

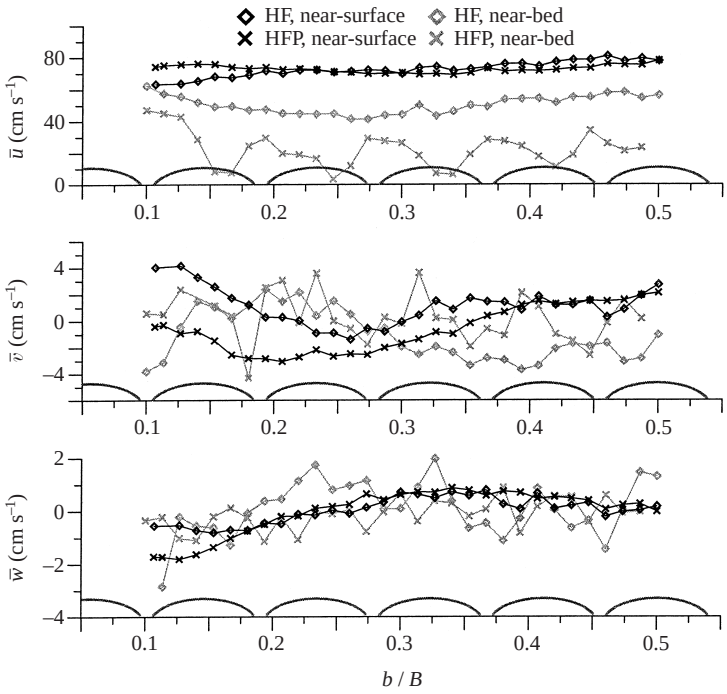

FIGURE 10. Transverse distribution of the mean velocities $\bar{u}$, $\bar{v}$, and $\bar{w}$. The measurement traverse is over roughness tops (figure 1*c*); b is the distance from the right-hand wall of the flume, and B is the flume width.

the 'periphyton' flows, i.e. it equals to the displacement length d established from the mean velocity and shear stress distributions. Above the roughness tops, periphyton does not affect the transport terms (figure 9). The $\overline{w'K}$-data for both flow types support the relationship $\langle\overline{w'K}\rangle/u_*^3 = 0.30$ recently suggested by Lopez & Garcia (1999) for the intermediate flow region in open-channel flows. The distribution of the mixed third-order moments in figure 9 strengthens the conclusion that the prevailing transport below the roughness tops occurs towards the flume bed, while above them the transport is upwards. The normalization of the mixed moments with the shear velocity and replacement of z with $(z-d)/(\Delta-d)$ nicely collapse the experimental points from both flow types.

4. Transverse distribution of turbulence properties and secondary currents

It is well known that in the near-wall regions of open-channel flows helical secondary currents are formed, which may significantly modify the distribution of the mean velocity and turbulence characteristics. Nezu & Nakagawa (1993) suggested that the width of the near-wall region, where secondary currents may be strong and so two-dimensional approximations are not valid, should be of order of 2.5 flow depths. The width to depth ratio B/H_a in our experiments was approximately 6.0–6.3 for the low flows and 4.3 for the high flows (table 1). With such low aspect ratios one would expect that quite a significant part of the flow should be occupied by helical secondary currents, and, thus, predictions for two-dimensional flows may be violated even in the central part of the flow. We have already pointed out that for all flows investigated the vertical distributions of the primary shear stress $-\langle\overline{u'w'}\rangle$ deviated

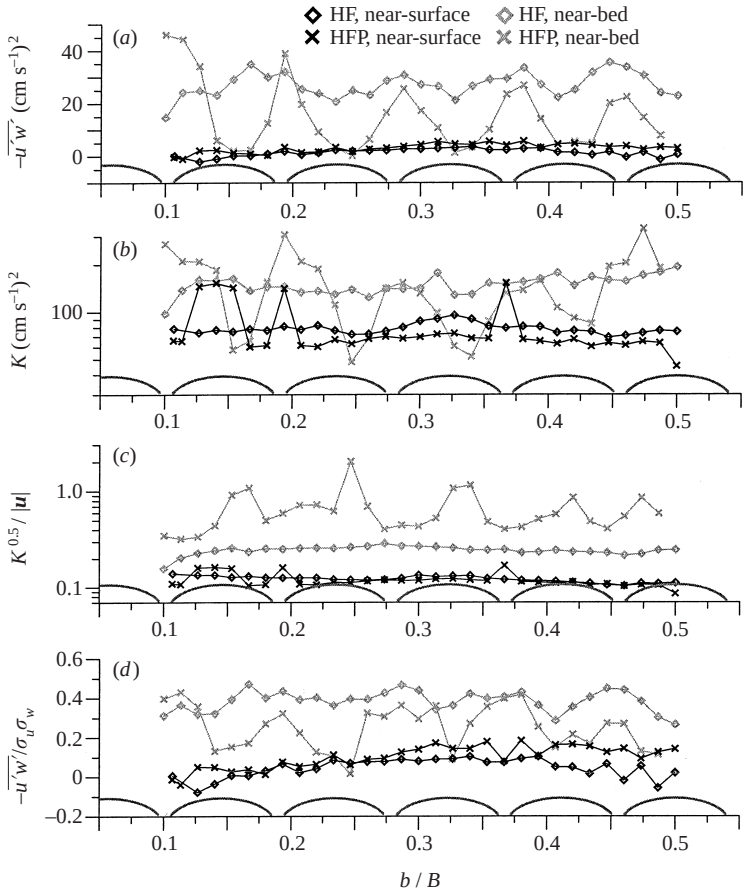

FIGURE 11. Transverse distribution of (*a*) the stress $-\overline{u'w'}$, (*b*) the total turbulence energy K, (*c*) the relative turbulence intensity $K^{0.5}/|\boldsymbol{u}|$, and (*d*) the correlation coefficient $-\overline{u'w'}/\sigma_u\sigma_w$. The measurement transverse is over roughness tops (figure 1); b is the distance from the right-hand wall of the flume, and B is the flume width.

from the predicted linear distribution (3). Data set 3 (figure 1*c*) allows us to identify the existence and extent of the helical secondary currents, to assess the effects of periphyton on their performance, and to evaluate the flow heterogeneity in the near-bed region due to spherical segments and the periphyton 'forelocks'. Figure 10 shows the transverse distributions of the local mean velocities $\bar{u}$, $\bar{v}$, and $\bar{w}$ in the near-bed and near-surface flow regions for high flows with and without periphyton on the bed. For both flow types, at least 30% of the flow width, adjacent to the wall, is occupied by secondary currents. Indeed, all three velocity components demonstrate behaviour typical for near-wall secondary currents (Nezu & Nakagawa 1993). Similar behaviour was also observed during hydraulic tests of this flume with the same 'velvet' coating of the bed surface but without the spherical segments (Nikora *et al.* 1998*b*). Although periphyton did not change the overall pattern in the distributions of $\bar{u}$, $\bar{v}$, and $\bar{w}$, it did change some specific properties. The most remarkable changes are an overall reduction in the near-bed longitudinal velocity $\bar{u}$ and its quasi-periodic transverse distribution, which is highly correlated with bed topography (figure 10). Interestingly, there was no strong correlation between the mean near-bed velocities and the bed top-

ography until periphyton 'forelocks' appeared on the tops of the spherical segments (compare figures 1 and 2). One can also note in figure 10 that the flow heterogeneity induced by the periphyton is much higher than that due to the secondary currents. The periphyton 'forelocks' affected not only the mean velocities but also the near-bed turbulence (figure 11). The primary Reynolds stress $-\overline{u'w'}$, the total turbulence energy K, and the correlation coefficient $-\overline{u'w'}/\sigma_u\sigma_w$ were appreciably enhanced in flow regions between the spherical segments and suppressed above their tops, similar to the longitudinal velocity in figure 10. In contrast, the relative turbulence intensity $K^{0.5}/|\boldsymbol{u}|$ was reduced between the segments and increased above the periphyton 'forelocks'. Thus, the appearance of periphyton 'forelocks' led to the local 'laminarization' of the flow above the spherical segments, and turbulence enhancement between them. The effect of periphyton on the near-surface flow properties was not so profound, as one would expect. Results for the low flows were similar.

5. Spatial velocity correlations, eddy convection, and velocity spectra

5.1. *Velocity correlations and eddy convection*

To evaluate the eddy convection velocity U_E we used the cross-correlation method:

$$U_E = \frac{\delta x}{\tau_{\max}}, \tag{5}$$

where $\tau_{\max}$ is the time lag in the cross-correlation function $R_i(\tau, \delta x)$ corresponding to the maximum ordinate of $R_i(\tau_{\max}, \delta x)$, δx is the distance between the measurement points 1 and 2 along the flow, i stands for velocity components 1 (u), 2 (v), or 3 (w), and $R_i(\tau, \delta x)$ is defined as $\overline{u_i'(x+\delta x, t+\tau)u_i'(x,t)}$. To explore the correlation function $R_i(\tau, \delta x)$, the dependence of U_E on distance from the bed, and to identify effects of periphyton on $R_i(\tau, \delta x)$ and U_E we used data set 2 (figure 1*b*). Figures 12(*a*) and 12(*b*) show typical correlation functions $R_u(\tau, \delta x)$ for the u velocity component, obtained from subset A (see figure 1*b*). As one can see, with the appearance of periphyton on the bed the maximum values of $R_u(\tau, \delta x)$ were reduced and, furthermore, periphyton de-correlated the velocity fluctuations below the roughness tops, though they were well-correlated in flows without periphyton. The correlation functions $R_v(\tau, \delta x)$ and $R_w(\tau, \delta x)$ show similar behaviour. Physically this means that in flows without periphyton the large-scale eddies, which are the main contributors to the maximum in $R_i(\tau, \delta x)$, successfully penetrate the interfacial sublayer and, thus, dominate in $R_i(\tau, \delta x)$. However, with periphyton on the bed the penetration processes are significantly weakened leading to velocity de-correlation within the interfacial sublayer. For both flow types the maximum values of $R_i(\tau, \delta x)$ quickly reduce with increase in δx, though still being detectable above the roughness tops at the largest δx used in our experiments (figure 1*b*). Figure 12(*c*) shows how the eddy convection velocity from (5) depends on the flow rate, the distance from the bed, and periphyton. In this figure, we use the mean values of U_E obtained by averaging corresponding values from $R_u(\tau, \delta x)$, $R_v(\tau, \delta x)$, and $R_w(\tau, \delta x)$. The figure shows that for both flow types, with periphyton and without, the ratio $U_E/\bar{u}$ increases towards the bed from ≈ 1 to 1.4–2.2, which is consistent with Nikora & Goring (2000*b*). Our data also suggest that the ratio $U_E/\bar{u}$ increases with increase in the flow rate and/or with the appearance of periphyton on the bed (figure 12*c*). The latter is probably due to the effect of displacement of the flow by periphyton.

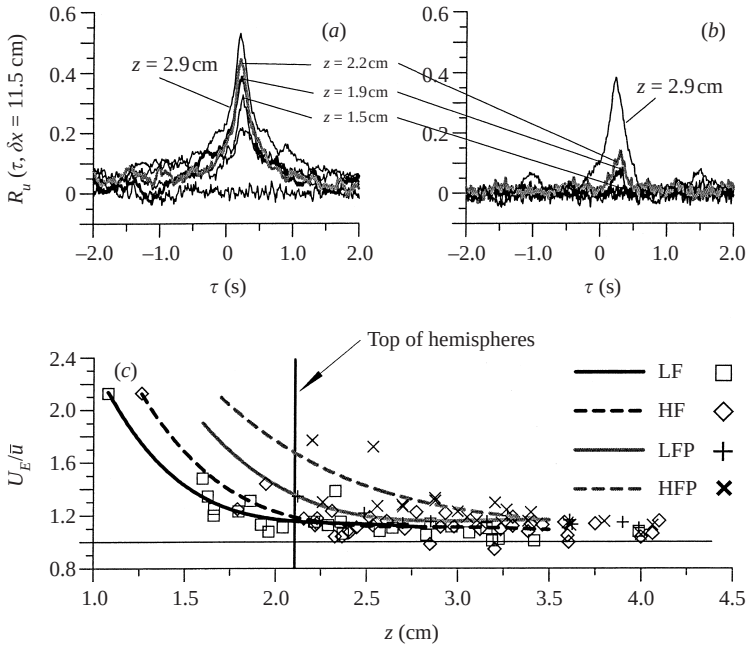

FIGURE 12. Correlation functions $R_u(\tau, \delta x = 11.5\,\text{cm})$ for the low flows (a) without periphyton and (b) with periphyton; and (c) the dependence of the eddy convection velocity U_E on the distance from the bed.

5.2. *Velocity spectra*

Figure 13(a) shows examples of frequency auto-spectra for the w velocity component at different locations and distances from the bed in low flow without periphyton. Near the bed (but above roughness tops) the auto-spectra demonstrate the existence of spectral ranges where $S_w(f) \propto f^{-1}$. With increase in z these ranges become narrower as the inertial subrange with $S_w(f) \propto f^{-5/3}$ expands towards the water surface. The auto-spectra for u and v (not shown here) behave in the same manner, though the range of the '−1' scaling is appreciably wider. Similar behaviour also occurs for the co-spectra $|C_{uw}(f)|$. At low frequencies the auto-spectra and co-spectra tend to constant values. The properties of the velocity spectra described here are in agreement with the four-range spectral model for open-channel flows (Nikora & Goring 1998*b*, 2000*a*; Nikora 1999). Below the roughness tops the spectra behave similarly, at least qualitatively (figure 13*a*). Note that the spectra in figure 13 are superposed with straight lines corresponding to $S_w(f) \propto f^{-1}$ and $S_w(f) \propto f^{-5/3}$ whose aim is two-fold: to show the applicability of $S_w(f) \propto f^{-1}$ and $S_w(f) \propto f^{-5/3}$, and to serve as benchmark lines so that differences in velocity spectra at different positions in the flow, as well as effects of periphyton, may be visually identified. The appearance of periphyton on the bed does not change appreciably the velocity spectra above the roughness tops although it significantly modifies them in the interfacial sublayer (figure 13*b*). The main modifications are: (i) reduction in the total spectral energy towards the flume bed (which one could predict using figure 6); and (ii) the appearance of a wide spectral peak with $f_{\max} \approx 3$ to 7 Hz. These new spectral features are also evident in the velocity spectra for the u and v velocity components and for both high and low flows, although the spectral peaks are not as strong as in the spectra of the vertical velocity. Estimates of the Strouhal number $Sh = f_{\max}\delta/\langle\bar{u}\rangle(\delta) \approx 0.09$–$0.20$, corresponding to

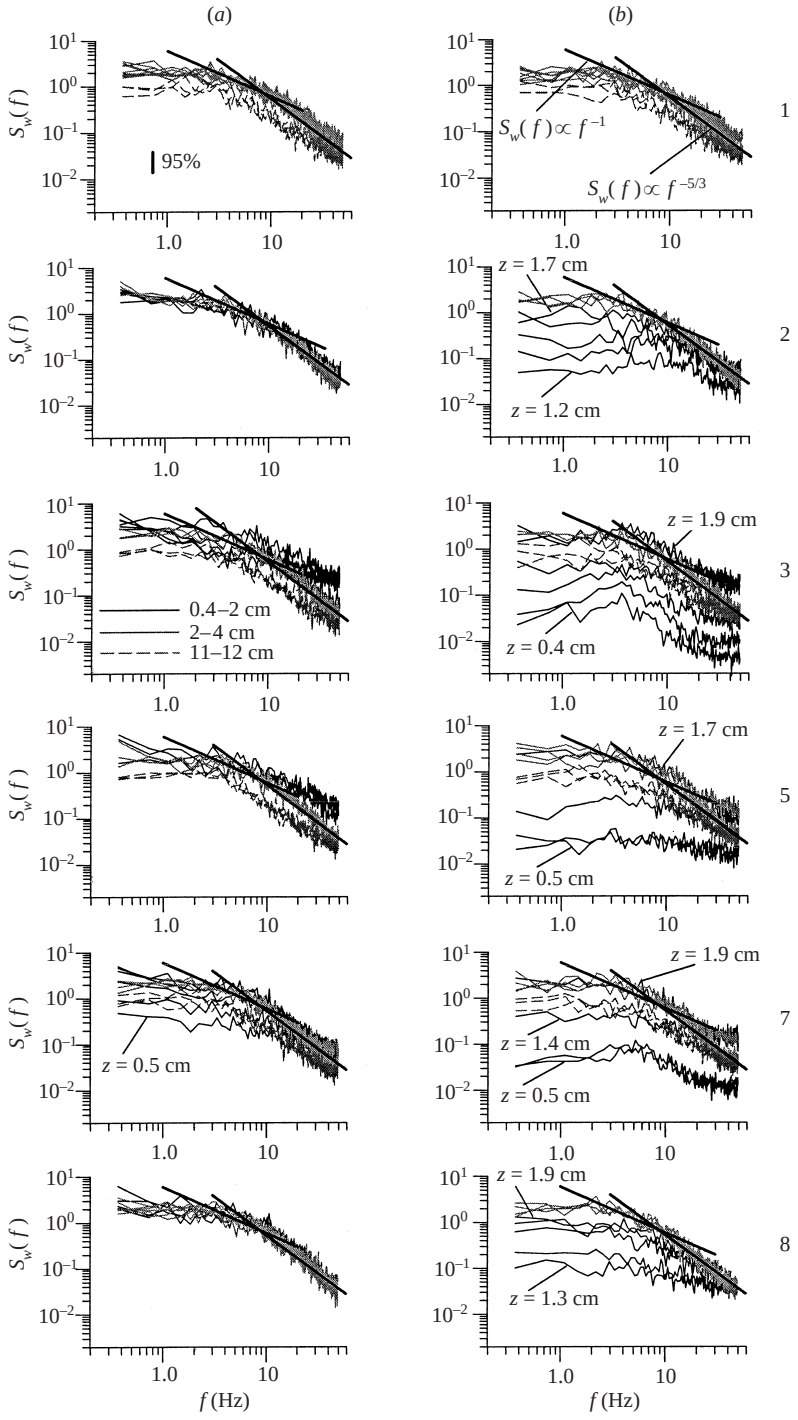

FIGURE 13. Examples of velocity auto-spectra for the vertical velocity component: (*a*) low flow without periphyton; and (*b*) low flow with periphyton. The numbers correspond to the ADV locations in figure 1(*a*).

the spectral peaks in figure 13(*b*), appeared to be two to three times lower than those for the model canopy in Brunet *et al.* (1994). The origin of the spectral peak at $f_{\max} \approx 3$ to 7 Hz is not yet clear. It can be either due to quasi-periodic flow separation from the spherical segments, triggered somehow by periphyton, or due to penetration of sweep events into the interfacial sublayer, 'filtered' by the periphyton 'forelocks'. We believe that the second explanation is more plausible as $f_{\max} \approx 3$ to 7 may correspond to the depth-scale eddies responsible for the sweep events. This explanation is also consistent with the fact that the spectral peaks at $f_{\max} \approx 3$ to 7 were more profound in the spectra of the vertical velocity. If our hypothesis is true, sweep events may be considered as the main mechanism responsible for the delivery of nutrients from the outer region to the biologically active interfacial sublayer.

6. Summary

The following flow properties and effects of periphyton–flow interactions were revealed in slightly accelerating, steady, nearly-equilibrium flows in an outdoor eco-hydraulic flume.

1. A linear velocity distribution in the interfacial sublayer and a logarithmic distribution above the roughness tops are reasonable approximations for both flow types, with and without periphyton on the bed. However, the appearance of periphyton on a rough bed shifted the origin of the bed upwards, increased the roughness length z_o by 16–21%, and reduced $C = \langle \bar{u} \rangle(\delta)/u_*$ by $\approx 30\%$. The effect of the flow rate on these parameters appeared to be insignificant (table 1).

2. The dispersive stresses as well as dispersive transport of the turbulence energy were negligible for both flow types. The main effect of periphyton on the vertical distribution of the stress $-\langle \overline{u'w'} \rangle$ is the nearly complete suppression of $-\langle \overline{u'w'} \rangle$ below $z = d$. The correlation coefficient $-\langle \overline{u'w'}/\sigma_u \sigma_w \rangle$ for both flow types, with and without periphyton, increases towards the bed, reaches a maximum at the level of the roughness tops, and then behaves differently, being larger for flows with periphyton on the bed (figure 4*e*). Approximate estimates showed that the shear production term appeared to be comparable with the wake production term, emphasizing the importance of both sources of turbulence energy generation near the rough bed.

3. Periphyton on the bed suppresses not only the mean velocities $\bar{u}$ and the stresses $-\langle \overline{u'w'} \rangle$ in the interfacial sublayer, but also turbulence intensities and vertical turbulent fluxes of the turbulent energy and the stress $-\overline{u'w'}$. However, their normalization with the shear velocity and replacement of z with $(z - d)/(\Delta - d)$ nicely collapse the experimental points for both flow types.

4. The transverse distribution of mean velocities and turbulence characteristics in our experiments clearly revealed near-wall helical secondary currents. However, the appearance of periphyton on the bed introduced quasi-periodic changes in flow properties with magnitudes much higher than the flow heterogeneity due to the secondary currents.

5. In flows without periphyton the large-scale eddies, which are the main contributors to the maximum in $R_i(\tau, \delta x)$, successfully penetrate the interfacial sublayer and, thus, dominate in $R_i(\tau, \delta x)$. However, periphyton 'forelocks' significantly weakened the penetration processes that led to velocity de-correlation within the interfacial sublayer.

6. The appearance of periphyton on the bed does not change appreciably the velocity spectra above the roughness tops but reduces the total spectral energy and generates a wide spectral peak with $f_{\max} \approx 3$ to 7 Hz in the interfacial sublayer. These

spectral properties are consistent with the analysis of $R_i(\tau, \delta x)$. We believe that the spectral peak revealed is due to the penetration of sweep events into the interfacial sublayer, 'filtered' by periphyton 'forelocks'. Thus, the sweep events may be the main mechanism responsible for the delivery of nutrients from the outer region to the biologically active interfacial sublayer.

7. The above points relate mainly to the effects of periphyton on the flow. However, the periphyton clearly felt the flow and we believe that the periphyton 'forelocks' are evidence of such a feedback. Indeed, initially the periphyton covered the bed surface uniformly, with approximately the same thickness (1–2 mm) on the spherical segments and between them. Then, transverse strips of quickly growing periphyton appeared on the spherical segments, and, finally, their tops were covered with periphyton 'forelocks' (figure 2). This phenomenon can be explained as follows. At the level of the roughness tops the mean velocities $\langle \bar{u} \rangle$ were higher than those in the interfacial sublayer below and, thus, the thickness of the viscous and diffusive sublayers around individual periphyton filaments on the tops of spherical segments were thinner. This lead to a higher rate of nutrient uptake by periphyton filaments and, thus, to a higher growth rate. With the appearance of the 'forelocks' the periphyton mat between the roughness elements became unstable, the mat thickness was reduced, and the periphyton mat became patchy. Our results suggest that this happened as a consequence of 'blocking' of the nutrient supply to the interfacial sublayer by the periphyton 'forelocks'.

These results have suggested several areas for future research that we are pursuing. First, the demonstrated importance of the displacement length d in collapsing the data with and without periphyton suggests that work should be done on how d can be evaluated in field conditions where the bed topography is irregular and the cobbles have a wide size distribution. Second, the implications of our results for the biota need to be assessed with more detailed biological studies involving species variety and abundance. Finally, we need to address the central question that stream biologists ask of their physics colleagues (Hart & Finelli 1999): what flow parameters should be measured to obtain the most appropriate quantification of the physical environment for stream biota?

This study was conducted under contracts CO1813 and CO1X0023 from the Foundation for Research Science and Technology (New Zealand). The authors are grateful to D. Hart for useful discussions, and S. Brown, R. Smith, and F. Munro for assistance with measurements and data analysis. Three anonymous reviewers provided thorough reviews and valuable comments which we gratefully incorporated into the final manuscript.

REFERENCES

Biggs, B. J. F. & Stokseth, S. 1996 Hydraulic habitat suitability for periphyton in rivers. *Regulated Rivers Res. Manage.* **12**, 251–261.

Biggs, B. J. F. & Thomsen, H. A. 1995 Disturbance of stream periphyton by perturbations in shear stress: link to structural failure and differences in community resistance. *J. Phycology* **31**, 233–241.

Bray, D. I. 1985 Flow resistance in gravel-bed rivers. In *Gravel-bed Rivers* (ed. R. D. Hey, J. C. Bathurst & C. R. Thorne), pp. 109–132. Wiley.

Brunet, Y., Finnigan, J. J. & Raupach, M. R. 1994 A wind tunnel study of air flow in waving wheat: single-point velocity statistics. *Boundary-Layer Met.* **70**, 95–132.

DITTRICH, A. & KOLL, K. 1997 Velocity field and resistance of flow over rough surface with large and small relative submergence. *Intl J. Sediment Res.* **12**, 21–33.

FINNIGAN, J. J. 1985 Turbulent transport in flexible plant canopies. In *The Forest–Atmosphere Interactions.* (ed. B. A. Hutchinson & B. B. Hicks), pp. 443–480. D. Reidel.

FINNIGAN, J. J. 2000 Turbulence in plant canopies. *Annu. Rev. Fluid Mech.* **32**, 519–571.

FINNIGAN, J. J. & MULHEARN, P. J. 1978 Modelling waving crops in a wind tunnel. *Boundary-Layer Met.* **14**, 253–277.

GIMENEZ-CURTO, L. A. & CORNIERO LERA, M. A. 1996 Oscillating turbulent flow over very rough surfaces. *J. Geophys. Res.* **101**(C9), 20745–20758.

GODILLOT, R. 1998 An experimental study of periphyton-flow interactions in a laboratory flume. PhD thesis, National Polytechnic Institute, Toulouse (in French).

GORING, D. G., NIKORA, V. I. & BROWN, S. L. R. 1998 ADVANS: A suite for turbulence analysis of ADV data. Manual. Part 1. *NIWA Internal Rep.* 11, 55 pp. NIWA, Christchurch.

GRIFFITHS, G. A. 1981 Flow resistance in coarse gravel bed rivers. *J. Hydraul. Div. ASCE* (HY) **7**, 899–918.

HART, D. D. & FINELLI, C. M. 1999 Physical-biological coupling in streams: the pervasive effects of flow on benthic organisms. *Annu. Rev. Ecol. Syst.* **30**, 363–395.

IZAKSON, A. 1937 Formula for the velocity distribution near a wall. *J. Exp. Theor. Phys.*, Russia, **7**, 919–924 (in Russian).

KAIMAL, J. & FINNIGAN, J. 1994 *Atmospheric Boundary Layer Flows.* Oxford University Press.

KRAUS, N. C., LOHRMANN, A. & CABRERA, R. 1994 New acoustic meter for measuring 3D laboratory flows. *J. Hydraul. Engng ASCE* **120**, 406–412.

LOHRMANN, A., CABRERA, R. & KRAUS, N. C. 1994 Acoustic Doppler velocimeter (ADV) for laboratory use. *Proc. Symp. on Fundamentals and Advancements in Hydraulic Measurements and Experimentation* (ed. C. A. Pugh). ASCE 351–365.

LOPEZ, F. & GARCIA, M. H. 1999 Wall similarity in turbulent open-channel flow. *J. Engng Mech. ASCE* **125**, 789–796.

MILLIKAN, C. B. 1939 A critical discussion of turbulent flows in channels and circula tubes. *Proc. 5th Intl Congr. Appl. Mech., Cambridge, MA*, pp. 386–392. Wiley.

MONIN, A. S. & YAGLOM, A. M. 1971 *Statistical Fluid Mechanics: Mechanics of Turbulence*, vol. 1. MIT Press.

MONIN, A. S. & YAGLOM, A. M. 1992 *Statistical Fluid Mechanics: Mechanics of Turbulence*, vol. 1. Gidrometeoisdat, St Petersburg, Russia (in Russian).

NEZU, I. & NAKAGAWA, H. 1993 *Turbulence in Open-Channel Flows.* A. A. Balkema.

NIKITIN, I. K. 1963 *Turbulent Channel flow and Processes in the Near-Bed Region.* Ukraine Acad. Sci., Kiev, Ukraine (in Russian).

NIKITIN, I. K. 1980 *Complex Turbulent Flows and Heat and Mass Transfer Processes.* Ukraine Acad. Sci., Kiev, Ukraine (in Russian).

NIKORA, V. I. 1999 Origin of the '−1' spectral law in wall-bounded turbulence. *Phys. Rev. Lett.* **83**, 734–737.

NIKORA, V. I. & GORING, D. G. 1998*a* ADV turbulence measurements: can we improve their interpretation? *J. Hydraul. Engng. ASCE* **24**, 630–634.

NIKORA, V. I. & GORING, D. G. 1998*b* Spectral scaling for gravel-bed open-channel flows. In *Stochastic Models of Hydrological Processes and their Applications to Problems of Environmental Preservations.* NATO Advanced Research Workshop, pp. 239–245. Water Problems Institute, Moscow, Russia.

NIKORA V. I. & GORING, D. G. 2000*a* Flow turbulence over fixed and weakly mobile gravel beds. *J. Hydraul. Engng ASCE* **126**(9), 679–690.

NIKORA, V. I. & GORING, D. G. 2000*b* Eddy convection velocity and Taylor's hypothesis of 'frozen' turbulence in a rough-bed open-channel flow. *J. HydroSci. Hydraul. Engng, JSCE* **18**(2), 75–91.

NIKORA, V. I., GORING, D. G. & BIGGS, B. J. F. 1997 On stream-periphyton-turbulence interactions. *NZ J. Mar. Freshwater Res.* **31**, 435–448.

NIKORA, V. I., GORING, D. G. & BIGGS, B. J. F. 1998*a* A simple model of stream periphyton-flow interactions. *Oikos* **81**, 607–611.

NIKORA, V. I., GORING, D. G. & BIGGS, B. J. F. 1998*b* Silverstream eco-hydraulic flume: hydraulic design and tests. *NZ J. Mar. Freshwater Research* **32**, 607–620.

NIKORA, V., GORING, D. MCEWAN, I. & GRIFFITHS, G. 2001 Spatially-averaged open-channel flow over a rough bed. *J. Hydraul. Engng ASCE* **127**(2), 123–133.

RAUPACH, M. R., ANTONIA, R. A. & RAJAGOPALAN, S. 1991 Rough-wall turbulent boundary layers. *Appl. Mech. Rev.* **44**, 1–25.

RAUPACH, M. R., COPPIN, P. A. & LEGG, B. J. 1986 Experiments on scalar dispersion within a model plant canopy. Part 1: The turbulence structure. *Boundary-Layer Met.* **35**, 31–52.

RAPAUCH, M. R. & SHAW, R. H. 1982 Averaging procedures for flow within vegetation canopies. *Boundary-Layer Met.* **22**, 79–90.

VOULGARIS, G. & TROWBRIDGE, J. H. 1998 Evaluation of acoustic Doppler velocimeter (ADV) for turbulence measurements. *J. Atmos. Ocean. Tech.* **15**, 272–289.

WILSON, N. R. & SHAW, R. H. 1977 A higher order closure model for canopy flow. *J. Appl. Met.* **16**, 1197–1205.